ORIGINAL ARTICLE

OPEN

Whole-Body ^{68}Ga-DOTANOC PET/MRI Versus ^{68}Ga-DOTANOC PET/CT in Patients With Neuroendocrine Tumors

A Prospective Study in 28 Patients

Dominik Berzaczy, MD,* Chiara Giraudo, MD,* Alexander R. Haug, MD,† Markus Raderer, MD,‡ Daniela Senn, BSc,† Georgios Karanikas, MD,† Michael Weber, PhD,* and Marius E. Mayerhoefer, MD, PhD*

Purpose: The aim of this study was to assess the diagnostic performance of simultaneous whole-body ^{68}Ga-DOTANOC PET/MRI compared with ^{68}Ga-DOTANOC PET/CT for detection of distant metastatic disease in patients with well-differentiated neuroendocrine tumors (NETs).

Methods: Patients with histologically proven, well-differentiated NET (G1 or G2) were included in this prospective, institutional review board–approved study. Patients underwent ^{68}Ga-DOTANOC PET/CT and subsequent ^{68}Ga-DOTANOC PET/MRI after a single tracer injection on the same day for staging or restaging purposes. Images were evaluated for the presence of NET lesions by 2 rater teams, each consisting of a nuclear medicine physician and a radiologist, in an observer-blinded fashion. Overall agreement, accuracy, sensitivity, and specificity, relative to a composite reference standard (consensus review including follow-up data), were calculated.

Results: Between July 2014 and June 2016, 28 patients were enrolled. Overall agreement and accuracy between the 2 rater teams were 91.7% (95% confidence interval [CI], 87.5%–95.9%) and 97% (95% CI, 94.4%–99.6%) for PET/MRI and 92.3% (95% CI, 88.3%–96.3%) and 94.6% (95% CI, 91.2%–98.1%) for PET/CT, respectively ($P = 1.00$).

Overall, PET/MRI reached 89.8% sensitivity (95% CI, 77.8%–96.6%) and 100% specificity (95% CI, 97%–100%); PET/CT showed 81.6% sensitivity (95% CI, 68%–91.2%) and 100% specificity (95% CI, 97%–100%) for the detection of metastatic disease in NETs.

Conclusions: Whole-body ^{68}Ga-DOTANOC PET/MRI appears to be comparable to ^{68}Ga-DOTANOC PET/CT for lesion detection in patients with well-differentiated NETs.

Key Words: ^{68}Ga-DOTA peptides, computed tomography, magnetic resonance imaging, neuroendocrine tumors, positron emission tomography

(*Clin Nucl Med* 2017;42: 669–674)

N euroendocrine tumors (NETs) are a group of fairly rare cancers that show a high degree of heterogeneity and disease complexity.[1]

These tumors originate from neuroendocrine cells, most commonly from the gastroenteropancreatic and bronchopulmonary system. An increasing incidence has been observed over the last decades, and disease-free survival is stagnate.[1–5] Metastatic disease has a high prevalence in this entity, predominantly in gastroenteropancreatic NET[6–8] (Fig. 1). In these patients, distant metastasis can be found in 38% to 50% at initial evaluation, particularly in the liver (Fig. 2) and lymph nodes.[5,6]

Chelator-conjugated somatostatin analogs labeled with ^{68}Ga (eg, DOTATATE, DOTANOC, and DOTATOC) due to a high affinity for somatostatin receptors (SSTRs) have an increased diagnostic accuracy over conventional imaging and Octreoscan in several studies.[9–11] Uptake of ^{68}Ga-DOTA peptides is very well correlated to the expression of SSTR type 2 in NETs, in particular, which allows sensitive diagnosis of well-differentiated NETs (G1 and G2) in ^{68}Ga-DOTA peptide PET/CT,[12,13] and quantification of SSTR expression; the latter also enables identification of patients who are eligible for peptide receptor radiotherapy with ^{177}Lu-DOTA peptides. In view of the literature, ^{68}Ga-DOTA peptide PET/CT is currently recommended as the imaging technique of choice by the European Neuroendocrine Tumor Society.[14]

Within the last few years, integrated PET/MRI scanners have become available for clinical use. While it is unlikely that PET/MRI will replace PET/CT in regular patient workup and clinical routine in the future, PET/MRI has certain advantages that may add useful information, because of the superior soft-tissue contrast of MRI, and furthermore the possibility of obtaining functional information when diffusion-weighted imaging (DWI) or dynamic contrast-enhanced imaging with hepatocellular contrast agents for detection of liver metastases is included in the MRI protocol. Nevertheless, in patients with NETs, it is unclear whether ^{68}Ga-DOTANOC PET/MRI is actually superior to ^{68}Ga-DOTANOC PET/CT, because of the high sensitivity (Se) and specificity (Sp) of the radiotracer itself.

The aim of the present, prospective study was therefore to assess the diagnostic performance of ^{68}Ga-DOTANOC PET/MRI compared with ^{68}Ga-DOTANOC PET/CT, for the detection of distant metastatic disease in patients with well-differentiated NETs.

PATIENTS AND METHODS

Patients and Study Design

Patients with histologically proven, well-differentiated NETs who were referred to our local tertiary care center for staging or posttherapeutic follow-up between July 2014 and June 2016 were consecutively enrolled in this prospective, institutional review board–approved study. Patients who gave written, informed consent underwent ^{68}Ga-DOTANOC PET/CT and, directly after that,
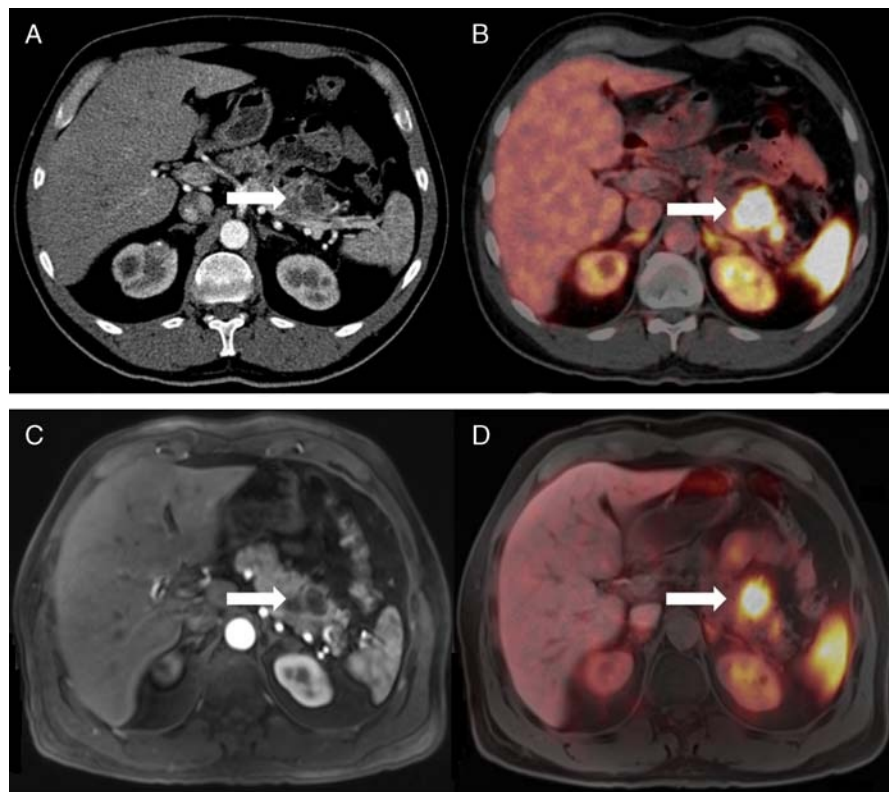
FIGURE 1. Primary NET (G1) in the body and tail of the pancreas (arrow) depicted in PET/CT (**A**, arterial contrast medium phase; **B**, corresponding fused PET/CT image) and in PET/MRI (**C**, T1 VIBE, arterial contrast medium phase; **D**, corresponding fused image) in a 46-year-old man.

^{68}Ga-DOTANOC PET/MRI. Pregnancy, general contraindications to MRI (eg, claustrophobia or metal or cochlear implants), and a known adverse reaction to iodinated contrast media served as exclusion criteria.

PET/MRI and PET/CT Protocols

^{68}Ga-DOTANOC PET/CT and ^{68}Ga-DOTANOC PET/MRI were performed consecutively on the same day, using a single tracer injection.

^{68}Ga-DOTANOC PET/CT was performed first, covering the anatomy from the vertex to the upper thigh, using a 64-multi–detector-row hybrid PET/CT device (Biograph TruePoint 64; Siemens, Erlangen, Germany). For PET, this scanner offers an axial field of view (FOV) of 216 mm, a sensitivity of 7.6 cps/kBq, and a transaxial resolution of 4 to 5 mm. PET was performed 45 to 60 minutes after an intravenous administration of approximately 165 MBq of ^{68}Ga-DOTANOC, with a 4-min/bed position, 4 iterations, and 21 subsets; a 5-mm slice thickness; and a 168×168 matrix, using the point-spread function–based reconstruction algorithm TrueX. Arterial-phase CT of the upper abdomen (ie, from the diaphragm to the lower pole of the kidneys) was acquired after the intravenous injection of 120 mL of a tri-iodinated, nonionic contrast medium at a rate of 4 mL/s. Venous-phase CT, which covered the entire anatomy, was used for attenuation correction. A tube current of 120 mA, a tube voltage of 230 kV, a collimation of 64×0.6 mm, a 5-mm slice thickness with a 3-mm increment, and a 512×512 matrix were applied.

^{68}Ga-DOTANOC PET/MRI, covering the same anatomy as the PET/CT, was performed directly after PET/CT (mean of 54 minutes between examinations), using an integrated, simultaneous, hybrid PET/MR device (Biograph mMR; Siemens) operating at 3 T, with

high-performance gradient systems (45 mT/m) and a slew rate of 200 T/m per second, and equipped with a phased-array body coil. For PET, the system offers an axial FOV of 256 mm, a sensitivity of 13.2 cps/kBq, and a transaxial resolution of 4.4 mm. PET was performed 100 to 150 minutes after the original tracer administration, with a 5-min/bed position, 3 iterations, and 21 subsets; a 4.2-mm slice thickness; and a 172×172 matrix, using the point-spread function–based reconstruction algorithm HD PET. A coronal, 2-point Dixon, 3-dimensional, volume-interpolated, T1-weighted (T1w) breath-hold MR sequence (VIBE) was acquired for attenuation correction using the following parameters: repetition time (TR)/echo time (TE) 3.6/TE1 = 1.23 milliseconds, TE2 = 2.46 milliseconds; 1 average, 2 echoes; a 10-degree flip angle; a 320×175 matrix with a 430×309-mm FOV; and a 3-mm slice thickness with a 0.6-mm gap. Axial, 3-dimensional, volume-interpolated, fat-suppressed, T1w breath-hold MR sequences (VIBE) were performed after contrast administration (ie, gadoxetic acid disodium [Gd-EOB-DTPA, gadoxetate], 2.5 mmol/kg followed by a saline flush of 20 mL/s), using the following parameters: TR/TE, 4.56/2.03 milliseconds; a 9-degree flip angle; a 195×320 matrix with a 380×309-mm FOV; and a 3-mm slice thickness with 0.6-mm gap; the dynamic contrast-enhanced series included arterial phase (postinjection delay, 22 seconds), venous phase (postinjection delay, 60 seconds), equilibrium phase (postinjection delay, 3 minutes), and a delayed hepatocyte-specific phase (postinjection delay, 20 minutes). The equilibrium phase was also obtained for the whole body. A coronal T2-weighted HASTE sequence was performed, with a TR/TE of 1400/121 milliseconds, a 160-degree flip angle, a 256×256 matrix with a 380×380-mm FOV, and a 6-mm slice thickness with a 1.2-mm gap. Average scan time for PET/CT was 30 ± 5 minutes (depending
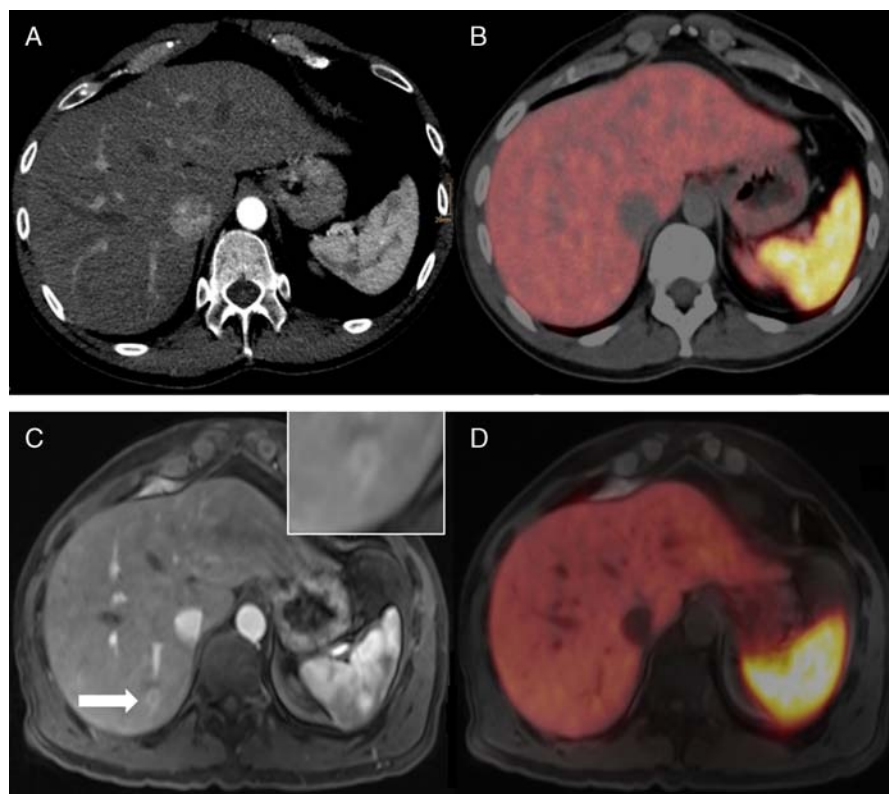
FIGURE 2. A 37-year-old man after surgically resected primary NET (G1) of the small bowel. In the arterial contrast medium phase in PET/CT (**A**), no focal liver lesion could be detected. In the corresponding fused PET images (**B**), no suspicious focal uptake was found in the liver parenchyma. PET/MRI revealed a small lesion in liver segment VI (**C**, T1 VIBE, arterial contrast medium phase) and focal uptake on the corresponding fused PET images (**D**).

on the PET acquisition time) and 50 ± 10 minutes for PET/MRI (depending on interindividual differences in respiratory gating).

Image Analysis

In the first step, 2 rater teams, each consisting of a board-certified nuclear medicine physician (A.R.H. with 13 years and G.K. with 15 years of experience in PET imaging, respectively) and a board-certified radiologist (D.B. with 4 ÿears and C.G. with 7 years of experience in oncologic imaging, respectively), performed the image analysis in consensus (ie, with side-by-side reading), blinded to the clinical information and the results of the analysis by the other rater team. The time interval between the evaluation of PET/MRI and PET/CT was 2 weeks. Primarily, liver, lung, bone, pleura, and lymph nodes were reviewed for metastatic disease. Additional findings (eg, other organ systems affected) were also recorded. To avoid organ bias, a maximum of 6 lesions were recorded per investigated region (anatomic site/organ).

On ^{68}Ga-DOTANOC PET/MRI, focal tracer accumulations, with any kind of morphological correlate on the T2-weighted or gadoxetate-enhanced T1w images, were rated as positive for the presence of a NET lesion. In addition, because of the limited spatial resolution of PET, lesions with marked contrast enhancement were rated as positive for NET, even if they did not show a clear tracer uptake. For liver lesions, early arterial enhancement with washout in the hepatocyte-specific delayed phase was used to confirm a metastatic lesion. Lesions with established benign MRI features, such as cysts, hemangiomas, or, for the liver, focal nodular hyperplasia, were rated as negative.

Similarly, on ^{68}Ga-DOTANOC PET/CT, focal tracer accumulations, with any kind of morphological correlate on arterial- or venous-phase CT, as well as PET-positive osseous lesions without anatomic CT correlate, were rated as positive for NET. Again, lesions with marked contrast enhancement were rated as positive for NET, whereas lesions with a benign enhancement pattern, such as hemangiomas and focal nodular hyperplasia, or cystic lesions with a lack of enhancement in combination with less than 20 Hounsfield units, were rated as negative.

In the second step, ^{68}Ga-DOTANOC PET/MRI and ^{68}Ga-DOTANOC PET/CT data were reevaluated by all 4 raters, and discrepancies were resolved in consensus. At this 4-rater consensus rating, SUVmax and SUVmean were also recorded for the largest lesion (ie, with the largest diameter) visible on both the PET component of the ^{68}Ga-DOTANOC PET/MRI and the PET component of the ^{68}Ga-DOTANOC PET/CT. This was done using isocontour volumes of interest that included all voxels greater than 50% of the SUVmax of each lesion and were constructed using the Syngo MultiModality Workplace environment (Siemens). In addition, SUV values were also measured for the liver and the mediastinal blood pool, by placing spherical volumes of interest with a 1-cm diameter in a lesion-free part of the liver parenchyma and the aortic arch, respectively.

Reference Standard and Statistical Analysis

The accuracy, agreement, Se, and Sp of ^{68}Ga-DOTANOC PET/MRI and ^{68}Ga-DOTANOC PET/CT, as well as their respective 95% confidence intervals (CIs), were first calculated independently

TABLE 1. Patient and Primary Tumor Characteristics

Age	
Mean age ± SD, y	62.1 ± 14.6
Sex, n	
Male/female (n = 28)	19/9
Localization of primary tumor, n	
Small bowel	15
Pancreas	7
Colon	2
Lung	1
Parotid paraganglioma	2
Unknown primary tumor	1
Total	28
Time to follow-up	
Mean age ± SD, mo	7.2 ± 4.2

for the 2 rater teams and subsequently for the unblinded 4-rater consensus evaluations.

Previous and/or follow-up examinations, together with pathohistological data from surgery or biopsy, if available, were used to generate a composite reference standard. Paired *t* tests were performed to compare SUVmax and SUVmean values measured on PET/MRI and PET/CT, respectively. The specified significance level was $P < 0.05$ for all tests. All statistical analyses were performed using IBM SPSS Statistics (version 22.0, IBM Corp, Armonk, NY).

RESULTS

Twenty-eight patients (19 male and 9 female patients; mean age, 62 ± 14 years) with NETs (G1, 11 patients; G2, 13 patients; in 4 patients, no grading was available because of the primary tumor localization [paraganglioma in 2 patients and lung carcinoid and cancer of unknown primary in 1 patient each]) fulfilled our inclusion criteria; no patients met the exclusion criteria. Pretherapeutic staging was the clinical indication for hybrid imaging in 5 patients, whereas 23 patients were referred to imaging for restaging. The primary NET was located in the intestine in 17 patients, in the pancreas in 7 patients, and in the parotid gland in 2 patients (paraganglioma); 1 patient showed a carcinoid of the lung, and in 1 patient, the primary disease site remained unknown (Table 1).

Blinded Rater Reading

For ^{68}Ga-DOTANOC PET/MRI, the 2 rater teams reached an overall agreement of 91.7% (95% CI, 87.5–95.9) compared with 92.3% (95% CI, 88.3–96.3) for ^{68}Ga-DOTANOC PET/CT (*P* = 1.00).

On PET/MRI, the 2 rater teams disagreed when judging lymph node involvement in 6 patients, for hepatic metastases in 4, for pancreatic lesions in 2, and for skeletal and pulmonary metastases in a single patient each. On PET/CT, we found discrepancies between our rater teams in 3 cases of lymph node and liver metastases, whereas for lung, skeletal, and pancreatic lesions, the 2 rater teams disagreed only in a single patient each. The Sp and Se for each rater team per organ/site can be found in Table 2.

Unblinded Consensus Reading

^{68}Ga-DOTANOC PET/MRI showed 100% Se and Sp for skeletal, hepatic, and lymph node metastases (Se 95% CI, 63.1%–100%, 80.5%–100%, and 76.8%–100%; and Sp 95% CI, 83.2%–100%, 71.5%–100%, and 76.8%–100%, respectively). Three pulmonary lesions and a pleural metastasis were missed by PET/MRI, resulting in 0% Se (95% CI, 0%–70.8% and 0%–97.5%, respectively) and 100% Sp (95% CI, 86.3%–100% and 87.2%–100%, respectively) for these sites. In ^{68}Ga-DOTANOC PET/CT, bone metastases were detected in 8 patients, whereas only 1 lesion (in a patient with 2 additional bone metastases) could not be detected (Se 87.5% [95% CI, 47.4%–99.7%]; Sp 100% [95% CI, 83.2%–100%]). Seventeen (60.71%) of 28 patients showed metastases in the liver. In 4 patients, 6 hepatic lesions were not detected (Se 76.5% [95% CI, 50.1%–93.2%]; Sp 100% [95% CI, 71.5%–100%]). Thirteen patients had involvement of lymph nodes, of which 5 nodes in 3 patients were false-negative (Se 78.6% [95% CI, 49.2%–95.3%]; Sp 100% [95% CI, 76.8%–100%]). All pulmonary and pleural metastases were correctly identified (Se 100%; Sp 100% each [Se 95% CI, 29.2%–100% and 2.5%–100%, respectively; Sp 95% CI, 86.3%–100% and 87.2%–100%, respectively). Among all other organs, in PET/MRI as in PET/CT, only 1 pancreatic lesion was not correctly identified (Se 83.3% [95% CI, 35.9%–99.6%]; Sp 100% [95% CI, 84.6%–100%], for each technique). An overview of Se and Sp per organ/site can be seen in Table 2.

SUVmax and SUVmean differed significantly ($P < 0.001$) between PET/CT and PET/MRI for measurements obtained from the mediastinal blood pool, liver parenchyma, and uptake in the largest detectable metastatic lesion (liver, 18; bone, 3; lymph node, 1; Table 3).

Overall, PET/MRI reached 89.8% Se (95% CI, 77.8%–96.60%) and 100% Sp (95% CI, 97%–100%), whereas PET/CT showed 81.6% Se (95% CI, 68%–91.24%) and 100% Sp (95% CI, 97%–100%) for the detection of metastatic disease in NETs. Overall accuracy for PET/MRI was 97% (95% CI, 94.4%–99.6%) and 94.6% for PET/CT (95% CI, 91.2%–98.1%).

DISCUSSION

In the present study, we compared the diagnostic performance of ^{68}Ga-DOTANOC PET/MRI to that of the standard hybrid imaging technique, ^{68}Ga-DOTANOC PET/CT in patients with

TABLE 2. Se and Sp per Rater and Organ/Site

	Rater Group 1		Rater Group 2		Consensus Reading	
	MRI	**CT**	**MRI**	**CT**	**MRI**	**CT**
Bone	100/100	87.5/100	87.5/100	75/100	100/100	87.5/100
Liver	76.5/100	58.8/100	100/100	76.5/100	100/100	76.5/100
Lymph nodes	71.4/100	78.6/100	85.7/100	42.9/100	100/100	78.6/100
Lung	0/100	66.7/100	0/100	100/100	0/100	100/100
Pleura	0/100	100/100	0/100	100/100	0/100	100/100
Other	66.7/100	66.7/100	100/100	83.3/100	83.3/100	83.3/100

Values (Se/Sp) are in %.

TABLE 3. SUVs for PET Components

	PET/CT			PET/MRI	
	SUVmax	SUVmean	*P*	SUVmax	SUVmean
Metastatic lesion	16.8 ± 9.8	8.9 ± 4.6	<0.001	11.6 ± 8.2	6.4 ± 3.9
Liver parenchmya	6.5 ± 2.5	4.8 ± 1.9	<0.001	4.4 ± 2.1	3.2 ± 1.3
Mediastinal blood pool	2.5 ± 0.7	1.4 ± 0.4	<0.001	2.1 ± 0.9	1.1 ± 0.6

Numbers are presented as mean ± SD.

well-differentiated NETs. Our study results indicate that the 2 techniques, PET/MRI and PET/CT, are generally equally useful in this particular setting, with a minor advantage for PET/MRI in terms of overall Se and accuracy, mainly due to an improved detection of liver metastases in the MRI component (Fig. 2). The only slight disadvantage for PET/MRI compared with PET/CT was for the detection of lung lesions. These findings are in good accordance with the results of previous studies that compared PET/MRI and PET/CT in different tumors and using different radiotracers.[15–21]

Notably, in patients with NETs, the liver is the primary solid organ target for metastases, as has been repeatedly shown in the literature,[22,23] and is also obvious when looking at lesion numbers in the present study (liver, 83 lesions in 17 patients; lungs, 6 lesions in 3 patients, according to our reference standard). For this reason, in our sequence protocol, we utilized gadoxetate-enhanced MRI, a technique that includes, apart from the standard contrast-enhanced phases (such as arterial, venous, and equilibrium phase), a hepatocyte-specific delayed phase, obtained 20 minutes after contrast-media injection. Gadoxetate-enhanced MRI is currently recognized as the most sensitive sequence for the detection of liver lesions, even ahead of DWI.[24] Despite the fact that we limited the maximum number of lesions per anatomic site/organ to 6, PET/MRI performed better than PET/CT in the detection of hepatic NET metastases. Thus, even though the overall performance of ^{68}Ga-DOTANOC PET/MRI and ^{68}Ga-DOTANOC PET/CT was comparable, PET/MRI may possibly be regarded as the hybrid imaging technique of choice for the evaluation of patients with NETs, as it is more sensitive in the most common site for organ metastases.

With the exception of gadoxetate-enhanced pulse sequences (obtained dynamically for the liver), our MRI protocol included only 1 additional, basic MR sequence (T2-weighetd HASTE), but no advanced sequences, such as DWI. This strategy was chosen because additional pulse sequences would have increased the total examination time considerably, thus affecting patient throughput. Patient throughput, in turn, is a critical issue for PET/MRI, which, together with higher device, installation, and maintenance costs, is one of the reasons why, from an economical point of view, PET/CT scanners are currently often regarded as a better investment than PET/MRI. With the present protocol, we were able to limit the total examination time of PET/MRI to a maximum of 45 minutes, which we believe is a fair compromise between speed and diagnostic information.

Our comparison of SUV data from ^{68}Ga-DOTANOC PET/MRI and ^{68}Ga-DOTANOC PET/CT clearly showed a small, albeit significant difference between the 2 techniques, with higher values measured on PET/CT than on PET/MRI. Similar comparative data have been reported in the literature for other tumors and tracers.[25,26] These differences between the 2 hybrid imaging techniques are thought to arise chiefly from the differences in attenuation correction methods (T1 VIBE Dixon for PET/MRI vs CT for PET/CT) but even more importantly due to the differences in scatter correction. The latter is of interest because an increased uptake at the delayed time point, as has been demonstrated for mucosa-associated

lymphoid tissue lymphomas,[27] might have been expected for NET, too. However, MALT lymphomas showed an increased uptake of ^{18}F-FDG—which is known to accumulate in malignant tumors over time—but not ^{68}Ga-DOTANOC. Therefore, scatter and attenuation correction, rather than the PET acquisition time point, is most probably the main reason for the observed SUV differences between PET/MRI and PET/CT. Notably, no lesion showed a focal tracer uptake in only 1 of the 2 imaging tests, even though the tracer washout in the surrounding tissue may have improved lesion-to-background PET contrast for the (delayed time point) PET/MRI.

Our study has several limitations. Apart from the rather small patient population, the fact that we included a considerable number of NET patients after surgery (22/28) limits our conclusions regarding the comparative performances of PET/MRI and PET/CT for the detection of primary NETs, which are most commonly found in the small bowel and the pancreas—hence, the focus of the present study was clearly on metastatic disease. However, this reflects the situation in routine clinical imaging of well-differentiated NETs, where—because of the slow growth of these tumors and the rather favorable prognosis in terms of survival—follow-up examinations are more common than pretherapeutic staging. Another limitation that our study shares with previous studies of similar design[24,28,29] is our use of a composite standard of reference for lesion verification, which was mostly based on previous imaging and follow-up examinations. While biopsies would have been the most reliable and thus preferable means of solving discrepancies between PET/MRI and PET/CT, this would not have been clinically feasible and would even have been unethical, as it would not have affected the management of any of these patients.

In conclusion, whole-body ^{68}Ga-DOTANOC PET/MRI and ^{68}Ga-DOTANOC PET/CT seem comparably accurate for the detection of well-differentiated NETs. The most likely advantage of PET/MRI, at least when the protocol includes gadoxetate-enhanced sequences, lies in the detection of liver metastases. Thus, for surgery planning in patients with known or suspected NET metastases of the liver, ^{68}Ga-DOTANOC PET/MRI may be preferable to ^{68}Ga-DOTANOC PET/CT.

REFERENCES

1. Yao JC, Hassan M, Phan A, et al. One hundred years after "carcinoid": epidemiology of and prognostic factors for neuroendocrine tumors in 35,825 cases in the United States. *J Clin Oncol*. 2008;26:3063–3072.
2. Modlin IM, Lye KD, Kidd M. A 5-decade analysis of 13,715 carcinoid tumors. *Cancer*. 2003;97:934–959.
3. Modlin IM, Oberg K, Chung DC, et al. Gastroenteropancreatic neuroendocrine tumours. *Lancet Oncol*. 2008;9:61–72.
4. Modlin IM, Moss SF, Chung DC, et al. Priorities for improving the management of gastroenteropancreatic neuroendocrine tumors. *J Natl Cancer Inst*. 2008;100:1282–1289.
5. Hallet J, Law CH, Cukier M, et al. Exploring the rising incidence of neuroendocrine tumors: a population-based analysis of epidemiology, metastatic presentation, and outcomes. *Cancer*. 2015;121:589–597.

6. Pavel M, O'Toole D, Costa F, et al. ENETS consensus guidelines update for the management of distant metastatic disease of intestinal, pancreatic, bronchial neuroendocrine neoplasms (NEN) and NEN of unknown primary site. *Neuroendocrinology.* 2016;103:172–185.

7. Frilling A, Modlin IM, Kidd M, et al.; Working Group on Neuroendocrine Liver Metastases. Recommendations for management of patients with neuroendocrine liver metastases. *Lancet Oncol.* 2014;15:e8–e21.

8. Niederle MB, Hackl M, Kaserer K, et al. Gastroenteropancreatic neuroendocrine tumours: the current incidence and staging based on the WHO and European Neuroendocrine Tumour Society classification: an analysis based on prospectively collected parameters. *Endocr Relat Cancer.* 2010;17:909–918.

9. Mojtahedi A, Thamake S, Tworowska I, et al. The value of (68)Ga-DOTATATE PET/CT in diagnosis and management of neuroendocrine tumors compared to current FDA approved imaging modalities: a review of literature. *Am J Nucl Med Mol Imaging.* 2014;4:426–434.

10. Haug AR, Cindea-Drimus R, Auernhammer CJ, et al. The role of ^{68}Ga-DOTATATE PET/CT in suspected neuroendocrine tumors. *J Nucl Med.* 2012;53:1686–1692.

11. Ruf J, Heuck F, Schiefer J, et al. Impact of Multiphase ^{68}Ga-DOTATOC-PET/CT on therapy management in patients with neuroendocrine tumors. *Neuroendocrinology.* 2010;91:101–109.

12. Haug AR, Assmann G, Rist C, et al. Quantification of immunohistochemical expression of somatostatin receptors in neuroendocrine tumors using ^{68}Ga-DOTATATE PET/CT. *Radiologe.* 2010;50:349–354.

13. Haug A, Auernhammer CJ, Wängler B, et al. Intraindividual comparison of ^{68}Ga-DOTA-TATE and ^{18}F-DOPA PET in patients with well-differentiated metastatic neuroendocrine tumours. *Eur J Nucl Med Mol Imaging.* 2009; 36:765–770.

14. Niederle B, Pape UF, Costa F, et al. ENETS consensus guidelines update for neuroendocrine neoplasms of the jejunum and ileum. *Neuroendocrinology.* 2016;103:125–138.

15. Sekine T, Barbosa FG, Sah BR, et al. PET/MR outperforms PET/CT in suspected occult tumors. *Clin Nucl Med.* 2017;42:e88–e95.

16. Afaq A, Fraioli F, Sidhu H, et al. Comparison of PET/MRI with PET/CT in the evaluation of disease status in lymphoma. *Clin Nucl Med.* 2017;42: e1–e7.

17. Melsaether AN, Raad RA, Pujara AC, et al. Comparison of whole-body (18)F FDG PET/MR imaging and whole-body (18)F FDG PET/CT in terms of lesion detection and radiation dose in patients with breast cancer. *Radiology.* 2016;281:193–202.

18. Souvatzoglou M, Eiber M, Takei T, et al. Comparison of integrated whole-body [^{11}C]choline PET/MR with PET/CT in patients with prostate cancer. *Eur J Nucl Med Mol Imaging.* 2013;40:1486–1499.

19. Lee SM, Goo JM, Park CM, et al. Preoperative staging of non–small cell lung cancer: prospective comparison of PET/MR and PET/CT. *Eur Radiol.* 2016;26:3850–3857.

20. Rauscher I, Eiber M, Fürst S, et al. PET/MR imaging in the detection and characterization of pulmonary lesions: technical and diagnostic evaluation in comparison to PET/CT. *J Nucl Med.* 2014;55:724–729.

21. Stolzmann P, Veit-Haibach P, Chuck N, et al. Detection rate, location, and size of pulmonary nodules in trimodality PET/CT-MR: comparison of low-dose CT and Dixon-based MR imaging. *Invest Radiol.* 2013;48:241–246.

22. Riihimäki M, Hemminki A, Sundquist K, et al. The epidemiology of metastases in neuroendocrine tumors. *Int J Cancer.* 2016;139:2679–2686.

23. McKenna LR, Edil BH. Update on pancreatic neuroendocrine tumors. *Gland Surg.* 2014;3:258–275.

24. Mayerhoefer ME, Ba-Ssalamah A, Weber M, et al. Gadoxetate-enhanced versus diffusion-weighted MRI for fused Ga-68-DOTANOC PET/MRI in patients with neuroendocrine tumours of the upper abdomen. *Eur Radiol.* 2013;23:1978–1985.

25. Eiber M, Takei T, Souvatzoglou M, et al. Performance of whole-body integrated ^{18}F-FDG PET/MR in comparison to PET/CT for evaluation of malignant bone lesions. *J Nucl Med.* 2014;55:191–197.

26. Jeong JH, Cho IH, Kong EJ, et al. Evaluation of Dixon sequence on hybrid PET/MR compared with contrast-enhanced PET/CT for PET-positive lesions. *Nucl Med Mol Imaging.* 2014;48:26–32.

27. Mayerhoefer ME, Giraudo C, Senn D, et al. Does delayed-time-point imaging improve ^{18}F-FDG-PET in patients with MALT lymphoma?: Observations in a series of 13 patients. *Clin Nucl Med.* 2016;41:101–105.

28. Hempel JM, Kloeckner R, Krick S, et al. Impact of combined FDG-PET/CT and MRI on the detection of local recurrence and nodal metastases in thyroid cancer. *Cancer Imaging.* 2016;16:37.

29. Grueneisen J, Schaarschmidt BM, Beiderwellen K, et al. Diagnostic value of diffusion-weighted imaging in simultaneous ^{18}F-FDG PET/MR imaging for whole-body staging of women with pelvic malignancies. *J Nucl Med.* 2014; 55:1930–1935.